Circuits Syst Signal Process (2016) 35:3380–3392
DOI 10.1007/s00034-015-0202-6

SHORT PAPER

Two Effective Strategies for Complex Domain Compressive Sensing

Ruirui Kang[1] · **Gangrong Qu**[1,3] · **Bin Wang**[2]

Received: 14 February 2015 / Revised: 2 November 2015 / Accepted: 3 November 2015 /
Published online: 13 November 2015

Abstract In this paper, we propose two novel recovery schemes for complex domain compressive sensing. Firstly, we present a new strategy to separate the real and imaginary parts of a complex signal for ℓ_1 minimization. While the method is simple, simulation results show that it is quite efficient because it reduces the sampling rate. Secondly, the least squares (LS) sub-problem is a key part of the orthogonal matching pursuit (OMP) algorithm and accounts for a large part of the computational load. We employ the Landweber algorithm to efficiently solve the LS problem. Furthermore, we propose four new parameter options to accelerate the convergence. Our numerical experiments show that our method is competitive with the pseudo-inverse.

Keywords Signal reconstruction · ℓ_1 minimization · Least squares · Landweber iteration · Orthogonal matching pursuit

Partially supported by the National Natural Science Foundation of China (61071144; 61271012).

✉ Gangrong Qu
grqu@bjtu.edu.cn

Ruirui Kang
11118381@bjtu.edu.cn

Bin Wang
15129884427@163.com

1 School of Science, Beijing Jiaotong University, Beijing 100044, China

2 Key Laboratory of Precision Opto-mechatronics Technology of the Ministry of Education, Beihang University, Beijing 100191, China

3 Beijing Center for Mathematics and Information Interdisciplinary Sciences, Beijing 100048, China

1 Introduction

Compressive sensing (CS) was first proposed in 2006 by Candès, Romberg, Tao [5,7], and Donoho [14]. Over the past 10 years, CS theory and applications have been developed extensively for domains such as quantum computing [18,23], radar [1, 30], compressive imaging [9,20], analog-to-information conversion [21,24], remote sensing [27,28,35], communications [11,12], and magnetic resonance imaging (MRI) [15,33]. CS is an efficient computational framework with powerful inference capability that provides insight into how a high-dimensional sparse signal can be reconstructed from a minimal number of measurements. It breaks the barriers of Nyquist sampling theory and recovers signals from just a few measurements under certain conditions.

Traditionally, CS has been performed on real-valued data. However, complex-valued data are very common in practical applications such as terahertz (THZ) imaging [8,25], synthetic aperture radar (SAR) [10], sonar (SAS) [19], and MRI [15,22,33]. CS reconstruction in this situation can benefit from extra information in the real and imaginary parts of the data. In this paper, our goal is to recover a sparse complex-valued signal $\mathbf{f} \in \mathbb{C}^{\mathbf{N}}$ from its measurement vector $\mathbf{y} = \boldsymbol{\Phi}\mathbf{f} \in \mathbb{C}^m$ with $m \ll N$, where $\mathbb{C}^N$ is represented as the N-dimensional complex domain and $\boldsymbol{\Phi} \in \mathbb{C}^{m\times N}$ denotes the complex-valued sensing matrix. This is achievable when the sensing matrix satisfies the restricted isometry property (RIP) [6]. In fact, the sensed measurement vector $\mathbf{y} \in \mathbb{C}^m$ consists of m random observations of the original signal and it comprises almost all of the information of the original data. The above-mentioned RIP is one of the most well-known properties of the sensing matrix $\boldsymbol{\Phi} \in \mathbb{C}^{m\times N}$, which ensures the exact reconstruction of the original sparse vector $\mathbf{f}$. We define two key notations to simplify the following discussions.

Definition 1 The support of a vector $\mathbf{f} \in \mathbb{C}^N$ is the index set of its nonzero entries:

$$\text{supp}(\mathbf{f}) := \{j \in [N] : f_j \neq 0\}. \tag{1}$$

where f_j is the *j-th* element of $\mathbf{f}$ and $[N] = 1, 2, \ldots, N$. The vector $\mathbf{f} \in \mathbb{C}^{\mathbf{N}}$ is *K-sparse* if at most K of its entries are nonzero, i.e., if

$$||\mathbf{f}||_0 = |\text{supp}(\mathbf{f})| \leq K, \tag{2}$$

where the ℓ_0 norm of a vector $||\mathbf{f}||_0$ is the number of nonzero entries in $\mathbf{f}$ and $|\text{supp}(\mathbf{f})|$ is the cardinality of $\text{supp}(\mathbf{f})$.

Definition 2 The restricted isometry constant δ_K of a matrix $\boldsymbol{\Phi} \in \mathbb{C}^{m\times N}$ is the smallest number such that

$$(1 - \delta_K)||\mathbf{f}||_2^2 \leq ||\boldsymbol{\Phi}\mathbf{f}||_2^2 \leq (1 + \delta_K)||\mathbf{f}||_2^2. \tag{3}$$

for all *K-sparse* vectors $\mathbf{f} \in \mathbb{C}^N$.

Random Fourier matrices are a very important class of structured random matrices that are suitable for practical applications. They were also the subject of study on CS

in [5,7]. A random partial Fourier matrix $\boldsymbol{\Psi} \in \mathbb{C}^{m\times N}$ can be constructed by randomly selecting m rows from the discrete Fourier matrix $\boldsymbol{\Psi} \in \mathbb{C}^{N\times N}$ with entries

$$\boldsymbol{\Psi}_{\omega,t} = e^{-2\pi i\omega t/N}, \quad \omega, t \in \{0, \cdots, N-1\}. \tag{4}$$

The partial random Fourier matrix was first proposed by Candès and Tao [5] and was improved by Rudelson and Vershynin [31]. The number of rows of the partial random Fourier matrix is recommended to be at least $m = \mathcal{O}(Klog^4(N))$, in which case the matrix would satisfy the RIP.

A natural and straightforward way to obtain a sparse solution from the underdetermined system $\mathbf{y} = \boldsymbol{\Phi}\mathbf{f}$ is formulated as the optimization problem of

$$\min_{\mathbf{f}\in\mathbb{C}^N} ||\mathbf{f}||_0 \qquad \text{subject to } \mathbf{y} = \boldsymbol{\Phi}\mathbf{f}, \tag{5}$$

which is an ℓ_0 optimization problem. Unfortunately, this combinatorial minimization problem is NP-hard. The problem in (5) is usually converted into ℓ_1 *minimization* by replacing $||\cdot||_0$ with its convex relaxation $||\cdot||_1$ as follows:

$$\min_{\mathbf{f}\in\mathbb{C}^N} ||\mathbf{f}||_1 \qquad \text{subject to } \mathbf{y} = \boldsymbol{\Phi}\mathbf{f}. \tag{6}$$

For a real-valued signal $\mathbf{f} \in \mathbb{R}^N$, Eq. (6) can be efficiently solved using various optimization algorithms such as proximal methods [26], primal-dual methods [34], and Bregman methods [17]. But in the complex-valued case, there are no existing direct methods to solve the problem in Eq. (6). In [5], a projected gradient descent algorithm is employed to reconstruct the original signal, but it requires at least eight times as many sampling points as the signal sparsity for a real-valued signal. A real-valued signal can be efficiently reconstructed from real measurement. However, this is inefficient for a complex signal. In fact, the ℓ_1-norm of a real vector equals to the sum of the absolute value of every component, while that of a complex vector is the square root of its real and imaginary parts [16]. Thus, the real and imaginary parts are unseparated [5], which leads to mutual interference and a requirement for more measurements to obtain sufficient information on the original signal. Reducing the number of sampling points is a crucial issue. We thus propose a new strategy for complex-valued CS. The main idea is to separate real and imaginary parts of complex variables to avoid the interference between them. Simulation results indicate that four times (for real signals) or six times (for complex signals) as many sampling points as the signal sparsity are sufficient for effective ℓ_1 minimization using our framework.

OMP is a practical and tractable method for the model in (5) [32] and has attracted attention for its competitive performance as well as its implementation simplicity and low computational complexity [13]. The main steps of OMP include matching and solving a LS sub-problem. For a complex signal, the square of its ℓ_2-norm is equal to the sum of the square of the signal comprised of its real and imaginary parts. There is no interference between its real and imaginary parts. Solving the LS sub-problem iteratively is the main computation load of OMP. To improve computational efficiency

of OMP, we use the Landweber algorithm to solve the LS sub-problem and propose four parameter options to accelerate the convergence of the Landweber algorithm.

The rest of the paper is organized as follows. The proposed strategy is introduced in Sect. 2. In Sect. 3, we present four parameter options. We present our simulation results in Sect. 4 and conclude this paper in Sect. 5.

2 Proposed Strategy

In this section, we present our proposed strategy for use in the ℓ_1 minimization method. $\boldsymbol{\Phi}^r$, $\mathbf{f}^r$, $\mathbf{y}^r$ and $\boldsymbol{\Phi}^i$, $\mathbf{f}^i$, $\mathbf{y}^i$ denote the real and imaginary parts of $\boldsymbol{\Phi}$, $\mathbf{f}$, $\mathbf{y}$, respectively, which can written as follows:

$$\begin{aligned} \mathbf{y} &= \mathbf{y}^r + j\mathbf{y}^i, \\ \boldsymbol{\Phi} &= \boldsymbol{\Phi}^r + j\boldsymbol{\Phi}^i, \\ \mathbf{f} &= \mathbf{f}^r + j\mathbf{f}^i, \end{aligned} \tag{7}$$

where j signifies the imaginary number. If $\mathbf{f}$ is a K-sparse complex signal, the sparsity level of its real part $\mathbf{f}^r$ and imaginary part $\mathbf{f}^i$ is both no more than K. That means that the real part $\mathbf{f}^r$ and imaginary part $\mathbf{f}^i$ of $\mathbf{f}$ are both K-sparse. We substitute Eq. (7) into the constrained equation $\mathbf{y} = \boldsymbol{\Phi}\mathbf{f}$ in Eq. (6) and obtain:

$$\begin{aligned} \boldsymbol{\Phi}^r\mathbf{f}^r - \boldsymbol{\Phi}^i\mathbf{f}^i &= \mathbf{y}^r, \\ \boldsymbol{\Phi}^i\mathbf{f}^r + \boldsymbol{\Phi}^r\mathbf{f}^i &= \mathbf{y}^i. \end{aligned} \tag{8}$$

This can be integrated as follows:

$$\mathbf{A}\mathbf{z} = \mathbf{b}. \tag{9}$$

where $\mathbf{A}$, $\mathbf{z}$, and $\mathbf{b}$ are defined as

$$\mathbf{A} = \begin{pmatrix} \boldsymbol{\Phi}^r & -\boldsymbol{\Phi}^i \\ \boldsymbol{\Phi}^i & \boldsymbol{\Phi}^r \end{pmatrix}, \quad \mathbf{z} = \begin{pmatrix} \mathbf{f}^r \\ \mathbf{f}^i \end{pmatrix}, \quad \mathbf{b} = \begin{pmatrix} \mathbf{y}^r \\ \mathbf{y}^i \end{pmatrix}. \tag{10}$$

where $\mathbf{z} \in \mathbb{R}^{2N}$, $\mathbf{A} \in \mathbb{R}^{2m\times 2N}$, and $\mathbf{b} \in \mathbb{R}^{2m}$. Then, Eq. (6) can be converted to

$$\min_{\mathbf{z}\in\mathbb{R}^{2N}} ||\mathbf{z}||_{\ell_1} \quad \text{subject to } \mathbf{A}\mathbf{z} = \mathbf{b}. \tag{11}$$

Obviously, Eq. (11) can be solved in the real domain. To solve it, two nonnegative slack vectors $\mathbf{u}$, $\mathbf{v} \in \mathbb{R}^{2N}$ are defined as

$$u_k = \begin{cases} z_k & if\ z_k > 0, \\ 0 & \text{otherwise}, \end{cases} \qquad v_k = \begin{cases} -z_k & if\ z_k < 0, \\ 0 & \text{otherwise}. \end{cases} \tag{12}$$

where u_k, v_k, and z_k are the *k-th* elements of $\mathbf{u}$, $\mathbf{v}$, and $\mathbf{z}$, respectively, and $\mathbf{z} = \mathbf{u} - \mathbf{v}$. The ℓ_1-norm of $\mathbf{z}$ can be represented as a linear function of $\mathbf{g} = [\mathbf{u}^T, \mathbf{v}^T]^T$, as

$$||\mathbf{z}||_1 = \mathbf{1}_{2N}^T(\mathbf{u} + \mathbf{v}) = \mathbf{1}_{4N}^T\mathbf{g}, \tag{13}$$

where $\mathbf{1}_{2N}$ is an all-ones vector with $2N$ elements. The constraint $\mathbf{Az} = \mathbf{b}$ can be represented as a linear function of $\mathbf{g}$

$$\mathbf{Az} = \mathbf{A}(\mathbf{u} - \mathbf{v}) = [\mathbf{A}, -\mathbf{A}]\mathbf{g}, \tag{14}$$

where $[\mathbf{A}, -\mathbf{A}] \in \mathbb{R}^{2m \times 4N}$. Therefore, the model in Eq. (6) can be converted to the following one:

$$\min \mathbf{1}_{4N}^T \mathbf{g} \qquad \text{subject to } [\mathbf{A}, -\mathbf{A}]\mathbf{g} = \mathbf{b}, \quad g_k \geq 0, \ k = 1, 2, \ldots, 4N. \tag{15}$$

The optimization problem in (15) can be efficiently solved by the primal-dual interior algorithm [2,4]. Given the solution $\bar{\mathbf{g}}$ of this program, the solution of (11) is recovered by

$$\bar{\mathbf{z}} = (\bar{g}_1 - \bar{g}_{2N+1}, \bar{g}_2 - \bar{g}_{2N+2}, \ldots, \bar{g}_{2N} - \bar{g}_{4N})^T. \tag{16}$$

Next, by integrating the real and imaginary parts of the complex variables (10), we obtain the reconstructed signal $\bar{\mathbf{f}}$ of the problem in Eq. (6) as

$$\bar{\mathbf{f}} = \bar{\mathbf{f}}^r + j\bar{\mathbf{f}}^i = (\bar{z}_1, \ldots, \bar{z}_N)^T + j(\bar{z}_{N+1}, \ldots, \bar{z}_{2N})^T.$$

3 Accelerated OMP

In the last section, we presented an algorithm for ℓ_1 minimization, which is a convex relaxation of ℓ_0 minimization. In this section, we introduce an accelerated OMP algorithm for ℓ_0 minimization. The OMP algorithm includes variable selection and LS optimization, and the entire process is described in Algorithm 1. Here, $\mathbf{x}_S$ is the sub-vector of $\mathbf{x}$ containing the elements of the support set S. $\boldsymbol{\Phi}^*$ represents the conjugate transpose of $\boldsymbol{\Phi}$, and $\boldsymbol{\Phi}_{S^n}$ is the sub-matrix whose columns correspond to the support set S^n.

Algorithm 1 OMP procedure

Input: Sensing matrix $\boldsymbol{\Phi}$, measurement vector $\mathbf{y}$;
Initial $\mathbf{x} \in \mathbb{C}^N$ (estimated sparse vector), $\mathbf{x}^0 = \mathbf{0}$, $\mathbf{r}^0 = \mathbf{y}$, $S = \emptyset$, $n = 0$;
repeat
$l_{n+1} := arg \max_{l \in [N]} \{|\boldsymbol{\Phi}^* \mathbf{r}^n|\}$;
$S^{n+1} := S^n \cup \{l_{n+1}\}$;
$\mathbf{x}^{n+1} := arg \min_{f \in \mathbb{C}^N} \{||\mathbf{y} - \boldsymbol{\Phi}\mathbf{f}||_2, \ \text{supp}(\mathbf{f}) \subset S^{n+1}\}$;
$\mathbf{r}^{n+1} := \mathbf{y} - \boldsymbol{\Phi}\mathbf{x}^{n+1} = \mathbf{y} - \boldsymbol{\Phi}_{S^{n+1}} \mathbf{x}_{S^{n+1}}^{n+1}$;
$n := n + 1$;
until $||\mathbf{r}^n|| \leq \varepsilon$ at $n = \bar{n}$;
Output: Approximate solution $\mathbf{f} = \mathbf{x}^{\bar{n}}$;

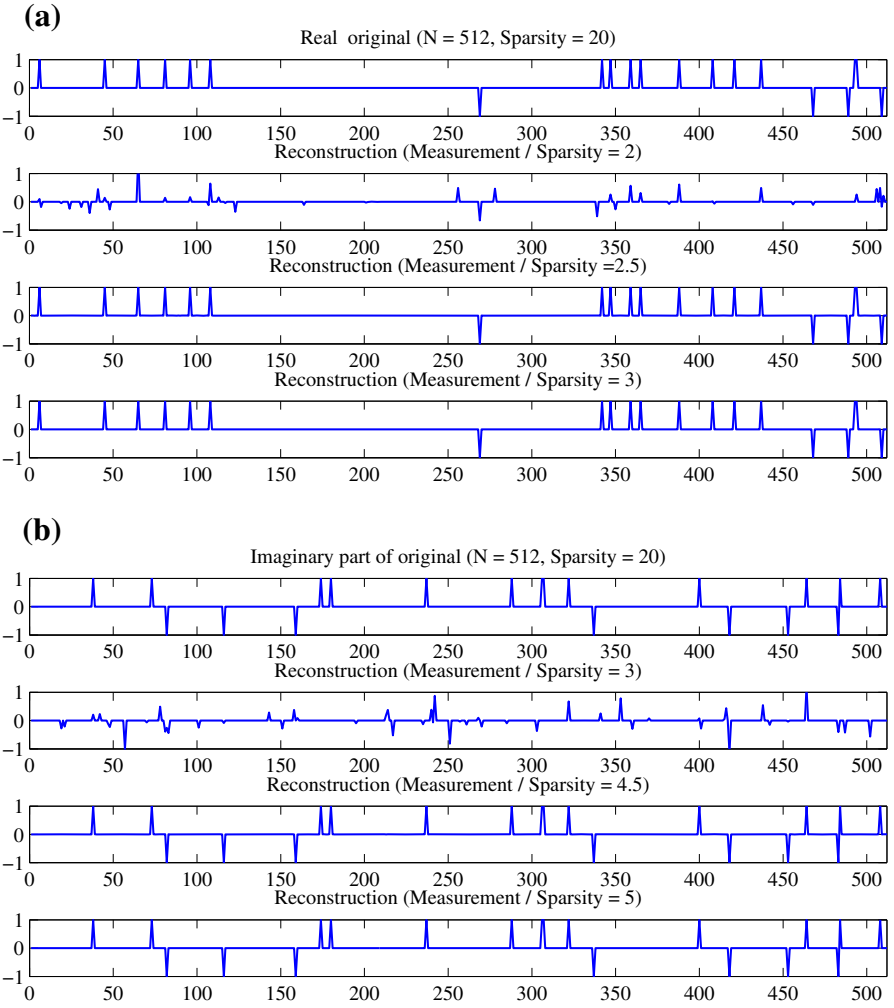

Fig. 1 **a**, **b** are recovered using the ℓ_1 minimization method with the proposed strategy for different numbers of measurements with fixed sparsity K. The *first rows* of (**a**) and (**b**) are the original real signal and the imaginary parts of the complex signal, respectively. The *other rows* are the reconstructions for the m/K values set to 2, 2.5, 3, and 3, 4.5, 5 from *top* to *bottom* in (**a**) and (**b**), respectively. **a** Real part of complex signal. **b** Imaginary part of complex signal

The LS optimization is the most computationally expensive part of the OMP algorithm and can be formulated as

$$\mathbf{x}^{n+1} := \arg\min_{\mathbf{f}\in\mathbb{C}^N}\{||\mathbf{y}-\boldsymbol{\Phi}\mathbf{f}||_2,\ \ \mathrm{supp}(\mathbf{f})\subset S^{n+1}\} \tag{17}$$

$$= \arg\min_{\mathbf{f}\in\mathbb{C}^N}\{||\mathbf{y}-\boldsymbol{\Phi}_{S^{n+1}}\mathbf{f}||_2\} \tag{18}$$

Tropp and Gilbert proved that OMP can ensure the accurate recovery of each fixed K-sparse signal from noise-free measurements with overwhelming probability [32], when $m \geq cK\log N$ is satisfied, where c is a constant.

Table 1 The relative errors of the real part and imaginary part of the signals

m/K	Real signal	Complex signal	
		Real part	Imaginary part
1	8.74888e−001	1.03417e+000	1.03267e+000
2	5.16207e−001	8.75185e−001	8.52343e−001
3	2.20812e−002	6.27557e−001	6.29275e−001
4	5.71156e−006	2.61904e−001	2.67823e−001
5	4.17394e−006	2.36945e−002	2.48317e−002
6	2.89869e−006	4.87386e−005	8.12898e−005
7	2.38584e−006	4.35414e−006	4.27679e−006
8	1.41942e−006	2.68140e−006	2.59874e−006

Because the main computational load in OMP is spent on solving the LS sub-problem, it is important to accelerate the LS sub-problem. The Landweber iteration requires a parameter that resembles step size in each iteration to solve $\boldsymbol{\Phi}_{S^n}\mathbf{f} = \mathbf{y}$ efficiently. This parameter is critical because it decides the convergence rate of the Landweber iterations. In this section, we present several parameter selection schemes to improve the performance of Landweber iteration. The Landweber algorithm [3] solves the system $\mathbf{y} = \boldsymbol{\Phi}\mathbf{f}$ using the following formula

$$\mathbf{f}^{k+1} = \mathbf{f}^k + \rho\boldsymbol{\Phi}^*(\mathbf{y} - \boldsymbol{\Phi}\mathbf{f}^k), \tag{19}$$

where ρ is a parameter. The Landweber iteration (19) is employed for the sub-problem $\boldsymbol{\Phi}_{S^n}\mathbf{f} = \mathbf{y}$, and the updating can be written as

$$\mathbf{f}^{k+1} = \mathbf{f}^k + \rho^k\boldsymbol{\Phi}_{S^n}^*(\mathbf{y} - \boldsymbol{\Phi}_{S^n}\mathbf{f}), \quad k = 1, 2, 3, \ldots. \tag{20}$$

The Landweber iteration (20) will converge when $0 < \rho^k < 2/\lambda_1$ is satisfied, where λ_1 is the largest eigenvalue of $\boldsymbol{\Phi}_{S^n}^*\boldsymbol{\Phi}_{S^n}$. It has been proven by Qu, Wang, and Jiang [29] that the range of parameters that ensure convergence is $[-1/\lambda_1, 3/\lambda_1]$. According to this, four ways to choose the parameter ρ^k, $k = 1, \ldots, r$, are as follows:

1. $\rho^k = 1/\lambda_1$.
2. $\rho^k = 2/(\lambda_1 + \lambda_r)$.
3. $\rho^k = 1/\lambda_k$, where λ_k is the *k-th* largest eigenvalue of $\boldsymbol{\Phi}_{S^n}^*\boldsymbol{\Phi}_{S^n}$.
4. $\rho^k = (1/\lambda_1 + q\triangle_\rho)$, $q = 0, 1, 2, \ldots, L-1$. L is a positive integer and $\triangle_\rho = (2/\lambda_1 - 1/\lambda_1)/L = 1/(\lambda_1 L)$.

The first case calculates the maximum eigenvalue of $\boldsymbol{\Phi}_{S^n}^*\boldsymbol{\Phi}_{S^n}$, and the second case calculates the maximum and minimum eigenvalues $\boldsymbol{\Phi}_{S^n}^*\boldsymbol{\Phi}_{S^n}$. The last case calculates the maximum eigenvalue of $\boldsymbol{\Phi}_{S^n}^*\boldsymbol{\Phi}_{S^n}$ and a constant step size which requires lower computational complexity than computing the other eigenvalues of $\boldsymbol{\Phi}_{S^n}^*\boldsymbol{\Phi}_{S^n}$. It is worth noting that the third method guarantees that the Landweber algorithm will converge within n iterations and this can be easily proved by Theorem III.1 in [29]. It is easy to verify that the ρ^k in the other methods are within the range of $[-1/\lambda_1, 3/\lambda_1]$

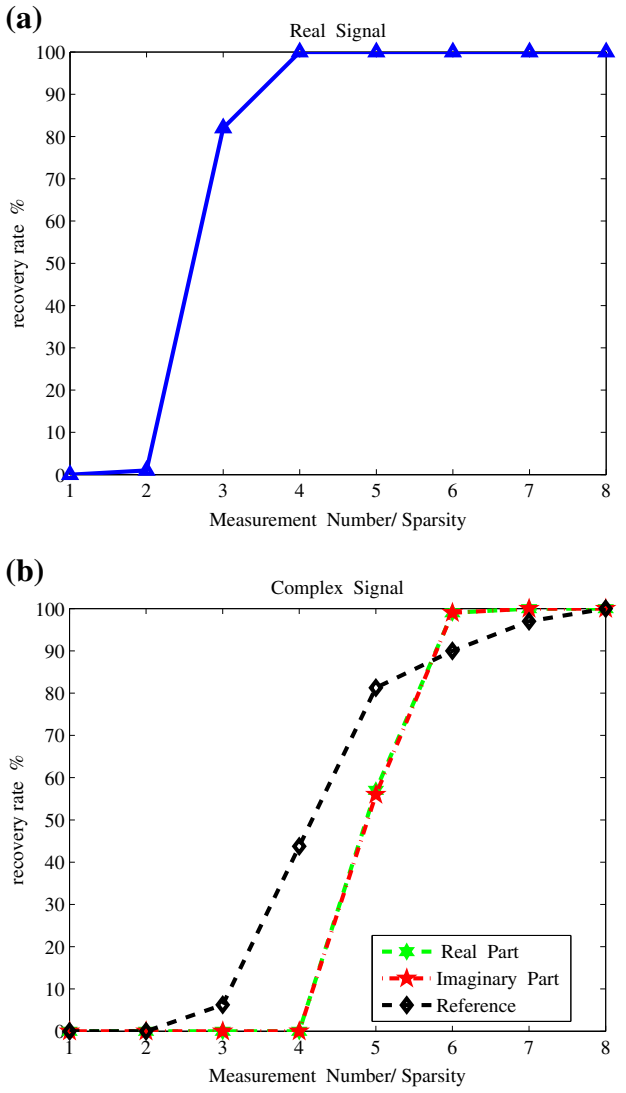

Fig. 2 Percentage of successful reconstructions of signal f as a function of m/K with varying numbers of measurements. **a** Performance for real signal. **b** Performance for complex signal

and ensure convergence. In addition, because of the RIP of the sensing matrix, the condition number of the sensing matrix is small and the OMP with the Landweber scheme is stable. These proposed methods are simpler than typical pseudo-inverse which needs to compute the singular value decomposition or QR decomposition of the related matrix.

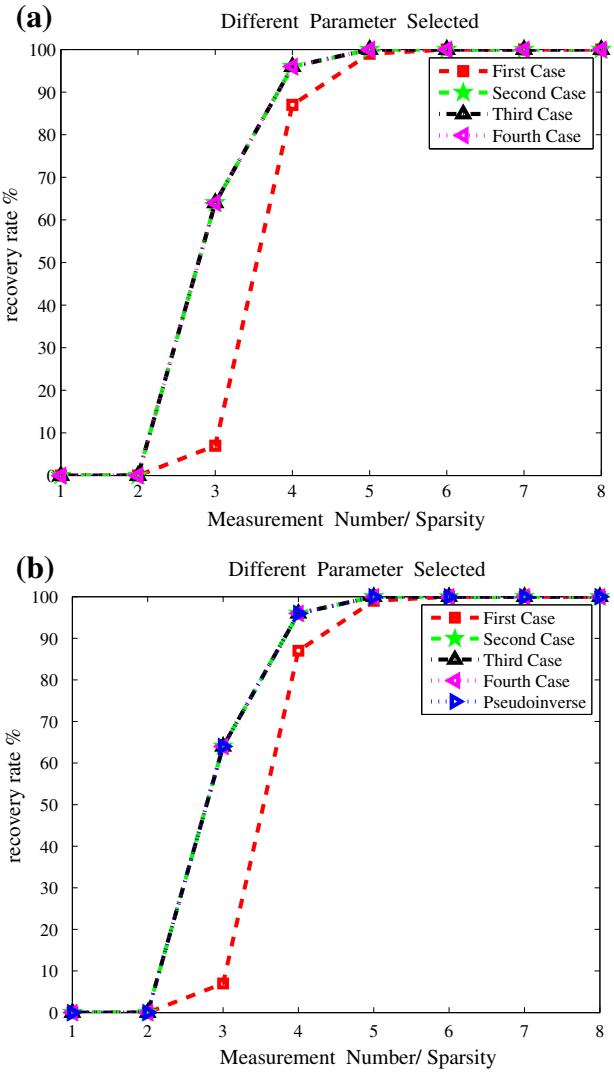

Fig. 3 Percentage of correctly recovered nonzero entries as a function of m/K for a complex signal using the OMP method with different parameter selection schemes to solve the LS problem. **a** Performance of the four parameter selection methods. **b** Performance of the four parameter selection methods and the pseudo-inverse

4 Experimental Results

In this section, we apply the two proposed algorithms on complex domain signal recovery by solving the problems in (6) and (17). Since there are no existing direct methods to solve problem (6) with a complex measurement matrix and complex signal, only the performance of the proposed algorithm is presented in the first subsection. Next,

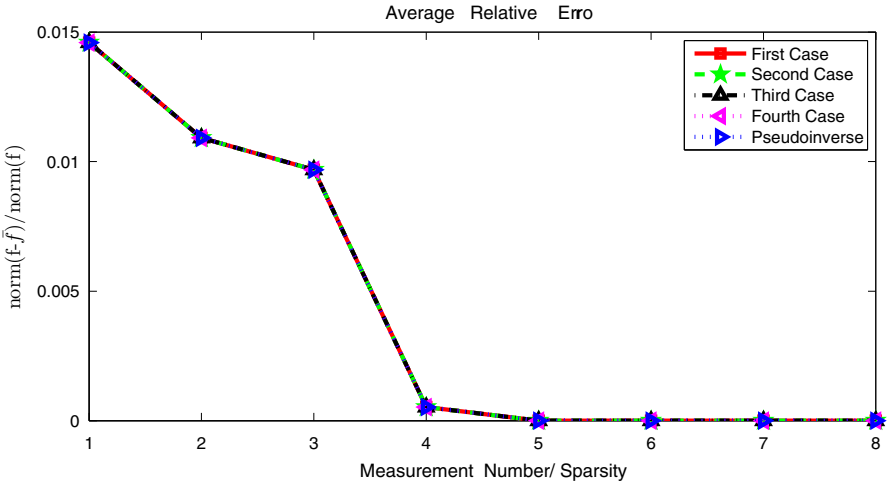

Fig. 4 The average RE as a function of m/K. The *curves* correspond to the mean of 100 trials

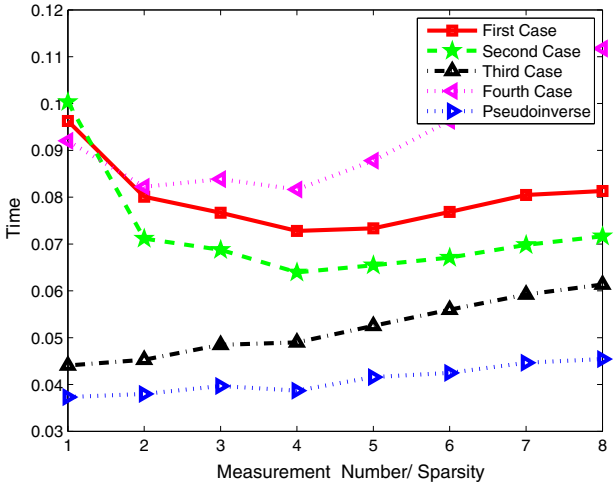

Fig. 5 The average time spent as a function of m/K. The *curves* correspond to the mean of 100 trials

the performance of the Landweber algorithm on the model in Eq. (17) is compared using different parameter options.

The main empirical task entails determining the minimal number of measurements m to recovery a K-sparse signal $\mathbf{f}$ with a high probability. Similar to [5], a random partial Fourier matrix $\boldsymbol{\Phi}$ of size $m \times N$ is generated by drawing m rows randomly from $N \times N$ ($N = 512$) discrete Fourier matrix $\boldsymbol{\Psi}$. The initial sensing matrix $\boldsymbol{\Phi}$ is generated independently for each trial. We generate K-sparse ($K = 20$) signal vector $\mathbf{f}$ whose nonzero locations are selected at random and the values of their real and imaginary parts follow the standard Gaussian distribution $\mathcal{N}(0, 1)$. It is assumed that the real and

imaginary parts of the input signal share a common support in the experiments. All experiments are run in MATLAB R2010a with a 2.40-GHz processor and 2GB RAM.

4.1 Performance of the Proposed Strategy for ℓ_1 Minimization Method

The performance of the proposed strategy for ℓ_1 minimization is demonstrated in Fig. 1. Here, for the recovery of real and complex K-sparse ($K = 20$) signals, the number of measurements is set to $m = 40; 50; 60$ and $m = 60; 90; 100$, respectively. As expected, the results show that the recovery accuracies increase with more measurements. It demonstrates that our method requires fewer measurements than [5] and provides an appropriate direct method for complex signal recovery. We use the relative error (RE) to evaluate the performance:

$$RE = \frac{||\bar{\mathbf{f}} - \mathbf{f}||_2}{||\mathbf{f}||_2}, \tag{21}$$

where $\bar{\mathbf{f}}$ is an estimation of the original K-sparse vector $\mathbf{f}$.

For each triple (K, m, N), we perform 100 independent trials in the following experiments. The average relative errors with varying numbers of measurements are listed in Table 1. As the value of m/K increases, the relative errors decrease, as expected.

Figure 2 presents another view of the same data. It displays the percentage of correctly recovered signals as a function of the value of m/K. For a fixed sparsity level K, the recovery probability increases with more measurements. The reference curve result is from [5] for comparison.

The data presented in Fig. 1, Table 1, and Fig. 2 demonstrate that the recovery rate of real and complex signals is 100% when $m \geq 4K$ and $m \geq 6K$. This indicates that the ℓ_1 minimization with our proposed strategy requires fewer sampling points than [5] which requires the number of sampling points to obey $m \geq 8K$.

4.2 OMP Based on the Landweber Algorithm

Here, we present the simulation results of our OMP approach based on the Landweber algorithm. We compare the performance of the Landweber algorithm using different parameter options to solve the LS sub-problem (17) in OMP. We set $K = 20$ and $N = 512$ and repeat 100 trials for each number of measurements $m \in \{20, 40, \ldots, 160\}$.

Figure 3 shows the recovery performance with different values of m/K. Clearly, higher m/K values correspond to better empirical reconstruction performance. The simulation results demonstrate that the overall behavior is the same for all four parameter settings except for the first case where the parameter ρ^k is set to the maximum eigenvalue of $\boldsymbol{\Phi}^*_{S^n}\boldsymbol{\Phi}_{S^n}$. For simplicity, the first case is employed in the following experiment.

Figure 4 shows the average RE for 100 independent trials. It can be observed that OMP based on the Landweber algorithm with four parameter options and the pseudo-inverse result in the same average RE value. Overall, the four parameter selection

approaches are competitive with the pseudo-inverse for solving the LS problem (17) in OMP.

Figure 5 shows the average time spent for the four parameter selection and the pseudo-inverse for 100 independent trials. As observed, the speed of the third parameter selection is the fastest and just slightly slower than the pseudo-inverse.

5 Conclusion

In this paper, we propose two algorithms for the complex domain CS problem. Firstly, a new strategy is proposed for ℓ_1 minimization by separating the real and imaginary parts of the partial Fourier matrix and the complex signal, to avoid interference between the different parts of complex variables. Numerical results demonstrate that the ℓ_1 minimization method requires fewer sampling points than [5] when applying the proposed method. Secondly, to efficiently solve the LS problem in OMP, we propose the Landweber algorithm with four parameter selection options. We compare the performance of the proposed method with the pseudo-inverse. Simulation results indicate that the performance of all four of our parameter selection approaches is equivalent to the classic pseudo-inverse.

References

1. R. Baraniuk, P. Steeghs, Compressive radar imaging. in *IEEE Radar Conference* (Waltham, Massachusetts, April 2007), pp. 128–133
2. S. Boyd, L. Vandenberghe, *Convex Optimization* (Cambrige University, Cambrige, 2004)
3. C. Byrne, *Iterative Algorithms in Inverse Problems* (University of Massachusetts Lowell Libraries, Lowell, 2006)
4. E.J. Candès, ℓ_1-MAGIC: recovery of sparse signals via convex programming. (2004) http://www-stat.stanford.edu/~candes/l1magic/
5. E.J. Candès, J. Romberg, T. Tao, Robust uncertainty principles: exact signal reconstruction from highly incomplete frequency information. IEEE Trans. Inf. Theory. **52**(2), 489–509 (2006)
6. E.J. Candès, T. Tao, Decoding by linear programming. IEEE Trans. Inf. Theory. **51**(12), 4203–4215 (2005)
7. E.J. Candès, T. Tao, Near optimal signal recovery from random projections: universal encoding strategies? IEEE Trans. Inf. Theory. **51**(12), 5406–5425 (2006)
8. W.L. Chan, M.L. Moravec, R.G. Baraniuk, D.M. Mittleman, Terahertz imaging with compressed sensing and phase retrieval. Opt. Lett. **33**(9), 974–976 (2008)
9. G. Coluccia, E. Magli, A novel progressive image scanning and reconstruction scheme based on compressed sensing and linear prediction. in *IEEE International Conference on Multimedia and Expo (ICME)* (Melbourne, Australia, July 2012), pp. 866–871
10. I. Cumming, F. Wong, *Digital Processing of Synthetic Aperture Radar Data* (Artech House, Norwood, 2005)
11. L. Dai, Z. Wang, Z. Yang, Compressive sensing based time domain synchronous OFDM transmission for vehicular communications. IEEE J. Sel. Area Commun. **31**(9), 460–469 (2013)
12. S. Das, T. Sidhu, Application of compressive sampling in synchrophasor data communication in WAMS. IEEE Trans Ind. Informat. **10**(1), 450–460 (2014)
13. J. Ding, L. Chen, Y. Gu, Perturbation analysis of orthogonal matching pursuit. IEEE Trans. Signal Process. **61**(2), 398–410 (2013)
14. D. Donoho, Compressed sensing. IEEE Trans. Inf. Theory. **52**(4), 1289–1306 (2006)
15. L. Fang, S. Li, R.P. Mcnabb, Q. Nie, A.N. Kuo, C.A. Toth, J.A. Izatt, S. Farsiu, Fast acquisition and reconstruction of optical coherence tomography images via sparse representation. IEEE Trans. Med. Imag. **32**(11), 2034–2049 (2013)

16. S. Foucart, H. Rauhut, in *A Mathematical Introduction to Compressive Sensing* (Birkhäuser, Boston, 2013)
17. T. Glodstein, S. Osher, The split Bregman method for L_1-regularized problem. SIAM J. Imaging Sci. **2**(2), 323–343 (2009)
18. D. Gross, Y.K. Liu, S.T. Flammia, S. Becker, J. Eisert, Quantum state tomography via compressed sensing. Phys. Rev. Lett. **105**(15) (2010) arXiv:0909.3304
19. M. Hayes, P. Gough, Synthetic aperture sonar: a review of current status. IEEE J. Ocean. Eng. **34**(3), 207–224 (2009)
20. H. Liu, B. Song, H. Qin, Z. Qiu, Dictionary learning based reconstruction for distributed compressed video sensing. J. Vis. Commun. Image. R. **24**(8), 1232–1242 (2013)
21. C. Luo, M.A. Borkar, A.J. Redfern, J.H. Mcclellan, Compressive sensing for sparse touch detection on capacitive touch screens. IEEE J. Emerg. Sel. Top. Circ. Syst. **2**(3), 639–648 (2012)
22. M. Lustic, D.L. Donoho, Sparse MRI: the application of compressed sensing for rapid MR imaging. Magn. Reson. Med. **58**(6), 1182–1195 (2007)
23. E. Magesan, A. Cooper, P. Cappellaro, Compressing measurements in quantum dynamic parameter estimation. (2013) arXiv:1308.0313v1
24. E. Matusiak, Y.C. Eldar, Sub-Nyquist sampling of short pulses. IEEE Trans. Signal Process. **60**(3), 3944–3947 (2012)
25. D. Mittleman, *Sensing with Terahertz Radiation* (Springer, Berlin, 2003)
26. N. Parikh, S. Boyd, Proximal algorithms. Found. Trends Optim. **1**(3), 123–231 (2013)
27. L. Poli, G. Oliveri, P. Rocca, A. Massa, Bayesian compressive sensing approaches for the reconstruction of two-dimensional sparse scatterers under TE illumination. IEEE Trans. Geosci. Remote Sens. **51**(5), 2920–2936 (2013)
28. L. Poli, G. Oliveri, F. Viani, A. Massa, MT-BCS-based microwave imaging approach through minimum-norm current expansion. IEEE Trans. Antennas Propag. **61**(9), 4722–4732 (2013)
29. G.R. Qu, C. Wang, M. Jiang, Necessary and sufficient convergence conditions for algebraic image reconstruction algorithms. IEEE Trans. Image Process. **18**(2), 435–440 (2009)
30. M. Rossi, A.M. Haimovich, Y.C. Eldar, Spatial compressive sensing for MIMO radar. IEEE Trans. Signal Process. **62**(2), 419–430 (2013)
31. M. Rudelson, R. Vershynin, Sparse reconstruction by convex relaxation: Fourier and Gaussian measurements. in *Proceedings of the 40th Annual Conference Information Sciences and Systems (CISS)* (Princeton, March 2006), pp. 207–212
32. J. Tropp, A. Gilbert, Signal recovery from random measurements via orthogonal matching pursuit. IEEE Trans. Inf. Theory. **53**(12), 4655–4666 (2007)
33. A. Webb, Magnetic resonance imaging. in *Introduction to Biomedical Imaging* (Wiley-Interscience, Hoboken, 2003), pp. 157–219
34. S.J. Wright, *Primal-Dual Interior-Point Methods* (SIAM, Philadelphia, 1997)
35. J. Yang, J. Thompson, X. Huang, T. Jin, Z. Zhou, Random-frequency SAR imaging based on compressed sensing. IEEE Trans. Geosci. Remote Sens. **51**(2), 983–994 (2013)